Cell Metabolism
Resource

Proteome Differences between Brown and White Fat Mitochondria Reveal Specialized Metabolic Functions

Francesca Forner,[1,3] Chanchal Kumar,[1,3,4] Christian A. Luber,[1] Tobias Fromme,[2] Martin Klingenspor,[2] and Matthias Mann[1,*]
[1]Department of Proteomics and Signal Transduction, Max Planck Institute for Biochemistry, 82152 Martinsried, Germany
[2]Molecular Nutritional Medicine, ZIEL Research Center for Nutrition and Food Sciences, Technische Universität München, Am Forum 5, 85350 Freising, Germany
[3]These authors contributed equally to this work
[4]Present address: Lilly Singapore Centre for Drug Discovery, 8A Biomedical Grove #02-05, Immunos, Biopolis 138648, Singapore
*Correspondence: mmann@biochem.mpg.de
DOI 10.1016/j.cmet.2009.08.014

SUMMARY

Mitochondria are functionally specialized in different tissues, and a detailed understanding of this specialization is important to elucidate mitochondrial involvement in normal physiology and disease. In adaptive thermogenesis, brown fat converts mitochondrial energy to heat, whereas tissue-specific functions of mitochondria in white fat are less characterized. Here we apply high-resolution quantitative mass spectrometry to directly and accurately compare the in vivo mouse mitochondrial proteomes of brown and white adipocytes. Their proteomes are substantially different qualitatively and quantitatively and are furthermore characterized by tissue-specific protein isoforms, which are modulated by cold exposure. At transcript and proteome levels, brown fat mitochondria are more similar to their counterparts in muscle. Conversely, white fat mitochondria not only selectively express proteins that support anabolic functions but also degrade xenobiotics, revealing a protective function of this tissue. In vivo comparison of organellar proteomes can thus directly address functional questions in metabolism.

INTRODUCTION

Mammals have two types of adipose tissue, brown (BAT) and white (WAT), which have different physiological roles and can be distinguished by their appearance and metabolic features (Cinti, 2005). The most important physiological function of BAT is nonshivering thermogenesis (NST), which is the primary thermogenic mechanism for small mammals and human neonates to prevent hypothermia (Klingenspor, 2003). Notably, recent data prove the presence of this tissue in healthy, adult humans (Nedergaard et al., 2007; Saito et al., 2009; van Marken Lichtenbelt et al., 2009; Virtanen et al., 2009). Brown adipocytes are very rich in mitochondria that uniquely express the uncoupling protein UCP1. When activated, this protein dissipates proton motive force in the form of heat. Controlled uncoupling is a potential strategy for the treatment of morbid obesity (Seale et al., 2009). UCP1 ablation induces obesity in mice kept at thermoneutrality (Feldmann et al., 2009).

White adipocytes are the major cellular components of visceral and subcutaneous WAT depots in humans (Cinti, 2005). However, in addition to being a fat reservoir, WAT is also an active endocrine organ that produces and secretes many signaling molecules, termed adipokines, which are involved in the regulation of food intake and energy homeostasis, and in the inflammatory states associated with metabolic disorders (Rosen and Spiegelman, 2006; Waki and Tontonoz, 2007). Thus WAT is involved in more diverse physiological processes than previously recognized.

Mitochondria play a central role in adipose metabolism, as highlighted by mitochondrial impairment in metabolic diseases (Crunkhorn and Patti, 2008; Holloway et al., 2009; Turner and Heilbronn, 2008) and neurodegenerative diseases, and in aging (Guarente, 2008; Katic et al., 2007). Thus it is clearly important to understand mitochondrial function in as much detail as possible.

Determining the mitochondrial proteome is a challenging task, which is made more difficult by the fact that mitochondria have versatile proteomes adapted specifically to diverse cellular and tissue requirements. Previously we used mass spectrometry (MS) to map mitochondrial proteomes qualitatively (Mootha et al., 2003) and semiquantitatively (Forner et al., 2006b) and uncovered tissue-specific traits based on protein presence or absence and on integration of measured peptide signals. Dramatically improved technology in quantitative MS-based proteomics now allow the measurement of relative protein abundances in biological samples with unprecedented precision (Cox and Mann, 2008; Mann and Kelleher, 2008).

Here we apply the stable isotope labeling by amino acids in cell culture (SILAC) technology to organellar studies (Andersen and Mann, 2006; Ong et al., 2002). In SILAC, cells grown in culture are metabolically labeled with either light or heavy amino acids, which makes the proteomes distinguishable in MS. The ratios of the peptides in MS directly yield the ratios of the proteins in the two cell states. We replace biochemical procedures at a preparative scale by first quantifying proteins in an enriched mitochondrial preparation against proteins enriched from other organellar preparations. Using this catalog of true mitochondrial proteins, we then achieve accurate quantitation of mitochondrial proteins in brown and white fat depots in vivo

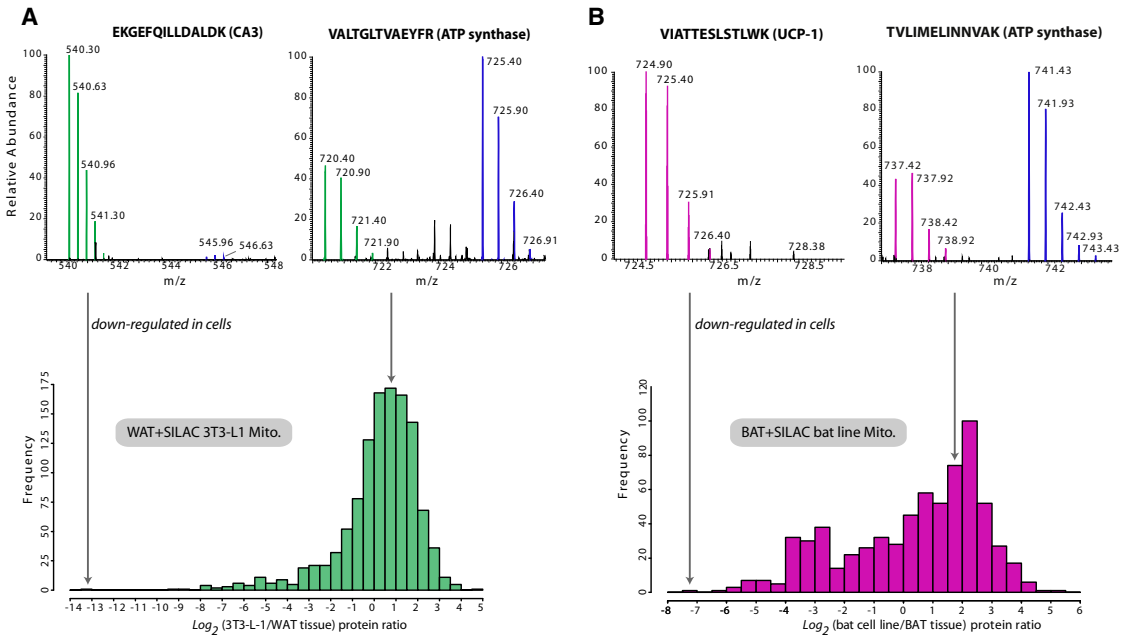

Figure 1. Brown and White Fat Cell Mitoproteomes In Vivo versus In Vitro

(A) MS spectra showing representative examples of proteins with different cell line-to-tissue ratios. The peptide signal in blue (on the right) is encoded in the heavy form and comes from the SILAC-labeled cell line. The peptide signals in green (on the left) are encoded in the light form and come from the WAT tissue. In the case of carbonic anhydrase (Ca3), only the light peptide peaks were detected (green); thus the protein was only present in tissue, whereas ATP synthase peptides were present in both light (green) and heavy forms (blue). On the lower part, the histogram represents the distribution of mitochondrial proteins obtained from inguinal fat depots and SILAC-labeled 3T3-L1 cells. The graphic represents protein frequency against the MS-measured protein ratios in vivo versus in vitro in log2 scale. (B) As above, with the histogram representing the distribution obtained from mitochondria of interscapular brown fat depots versus mitochondria isolated from a cell line of brown adipocytes. UCP1 was only detected in tissue mitochondria, whereas ATP synthase was present in both tissue (peptide in red) and cell line (peptide in blue).

by using SILAC-labeled mitochondrial proteins as internal references. By mapping accurate protein level ratios in BAT against WAT to metabolic pathways, we uncover molecular determinants of divergent metabolic activities in these fat types. We find that mitochondria in fat tissues express unique protein isoforms and entire pathways on a cell-type-specific basis. Finally, we analyze the response of the mitochondrial proteome to cold-induced thermogenesis, a specialized function of brown fat that increases energy expenditure.

RESULTS

Fat Cell Line Mitochondria versus In Vivo Mitochondria

We initially SILAC labeled the white fat cell line 3T3-L1 and a cell line of brown adipocytes. We noticed that prominent tissue-specific mitochondrial proteins, such as the uncoupling protein UCP1, were not detected by MS despite in depth coverage of the proteome. While UCP1 may only be expressed in cell culture upon stimulation (Ross et al., 1992), it was readily detected in vivo (see below). The low abundance of this and other major markers in cultured adipocytes prompted us to develop an in vivo analysis strategy, which preserves the precision of quantitation achievable with SILAC-labeled cells, and to characterize proteomic differences between tissue and cultured adipose cells at the mitochondrial level.

We SILAC labeled 3T3-L1 cells to completion with heavy forms of arginine and lysine and isolated mitochondria. In parallel, we extracted mitochondria from adipose cells of epididymal fat depots. The two populations were mixed one to one and analyzed by high-resolution MS on a LTQ-Orbitrap instrument. If cell line and in vivo proteomes were quantitatively very similar, fold-change histograms of protein ratios between cell line and tissue would be a narrow, symmetrical distribution around the one-to-one ratio. Most proteins indeed follow a roughly Gaussian distribution, although their relative levels differ up to 6-fold and some proteins are much more represented in tissue than in cell culture (Figure 1A, see Table S1 available online).

We also labeled a brown adipocyte cell line, isolated mitochondria, and compared their proteome with the mitochondrial proteome of adipose cells isolated from interscapular brown fat depots (Figure 1B). We found a substantial subset of proteins whose expression is severely downregulated in the cell line, including UCP1, subunits of Complexes I and III, and several other proteins involved in lipid metabolism (Table S1). The substantial differences between mitochondria of cell lines and tissue, especially in the case of brown adipocytes, prompted us to directly analyze the tissue mitochondrial proteomes.

The In Vivo Mitochondrial Proteome of Brown and White Fat Cells

Here we develop an organellar proteomics approach that does not require high purity of the target organelle as achieved in gradient centrifugations (Andersen and Mann, 2006; Yates et al., 2005). We use crude organellar preparations (e.g.,

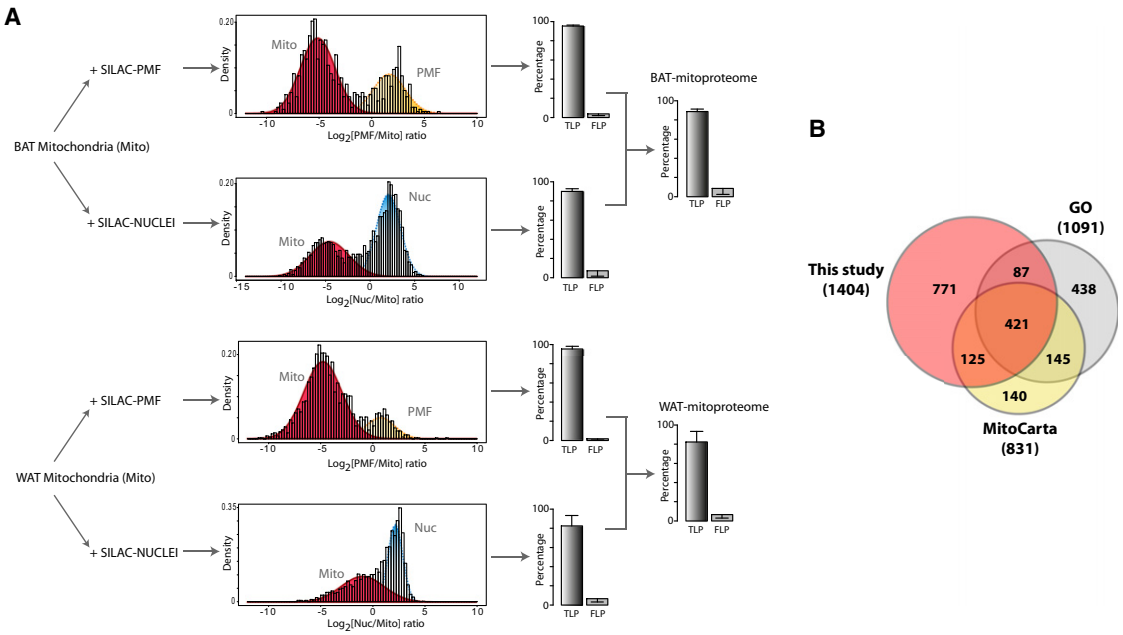

Figure 2. Quantitative Proteomics Defines Mitochondrial Localization

(A) Protein ratio distributions obtained by mixing mitochondria from brown fat depots with nuclear and postmitochondrial fractions enriched from SILAC-labeled brown adipocytes. TLP and FLP are metrics that determine the performance of the mitochondrial localization approach (Experimental Procedures). The metrics are shown for the two separate experiments and for the union. The positive error bars for the TLPs show the improvement by including "BORDER" localized proteins. The negative error bars for the FLPs show the decrease in the metric by factoring multiple GO subcellular localization in addition to mitochondrial localization (Table S3). Below, the plotted distributions represent mitochondria from white fat depots, and nuclear and postmitochondrial fractions from SILAC-labeled 3T3-L1.

(B) Venn diagram showing the overlap of our adipose mitochondrial proteome with GO-annotated mitochondrial proteins and with adipose tissue proteins mapped to mitochondria in MitoCarta.

mitochondria) and mix them with SILAC-labeled fractions that are enriched with other organellar fractions representing the background. We make use of the fact that genuine mitochondrial proteins must show differential SILAC ratios when comparing a mitochondrial enriched fraction to other crude fractions. Our method can be conveniently applied where classical biochemical methods are precluded due to limited material or due to unwanted loss of proteins that are loosely associated to the organelle or structure of interest.

As background fractions to quantify the enrichment, we used crude fractions from the labeled cell lines. First we isolated nuclear (Nuc) and soluble postmitochondrial (PMF) fractions from SILAC-labeled brown adipocytes and 3T3-L1 cell lines. We then separately mixed these fractions with mitochondria isolated from brown and white adipose tissues in a 1:1 ratio and measured the samples by high-resolution MS. The SILAC-protein ratios (PMF/Mito and Nuc/Mito) between subcellular fractions then allow distinguishing mitochondrial proteins from background populations. A histogram of the protein ratios for BAT revealed a bimodal pattern with the left distribution (low PMF/Mito ratios) containing the mitochondrial proteins (Figure 2A). Likewise, mitochondrial proteins separated from nuclear contaminations by ratios in the Nuc/Mito experiment. The same two experiments were performed for WAT tissue (Figure 2A).

To extract a reliable core of mitochondria-localized proteins, we adopted a probabilistic model based on Bayesian inference to assign localization probabilities to proteins based on their SILAC ratios. We first assumed that the ratio patterns originated from two distinct Gaussian distributions and used the expectation maximization (EM) algorithm (Dempster et al., 1977) to train the fitting. Second, we assigned a probabilistic index to each protein to estimate its localization (Supplemental Experimental Procedures and Table S2). To evaluate the accuracy of our method, we quantified the percentage of true and false localizations and used the Gene Ontology (GO) cellular compartment annotation as benchmark (Ashburner et al., 2000) (Table S3).

Across the four experiments, the fraction of mitochondrial proteins assigned concordantly with GO varied from 83% (in WAT Nuc versus Mito) to 95% (in both PMF versus Mito) and was consistently higher in the PMF versus Mito cases, probably due to trafficking of proteins between nuclei and mitochondria (Ryan and Hoogenraad, 2007) resulting in copurification. Mitochondrial proteins classified as nonmitochondrial were between 2% (WAT PMF versus Mito) and 7% (in both Nuc versus Mito). False mitochondrial localization was only 0.5% when considering proteins annotated exclusively as mitochondrial in GO.

After consolidating the localization assignments across all experiments, we assigned 723 mitochondrial proteins in BAT and 1198 in WAT. Together, we obtained a BAT and WAT in vivo adipose mitochondrial proteome of 1404 proteins—significantly extending our knowledge of mitochondria-associated proteins in fat cells.

We then compared our consolidated adipose mitoproteome with GO-annotated mitochondrial proteins (1091 IPI identifiers)

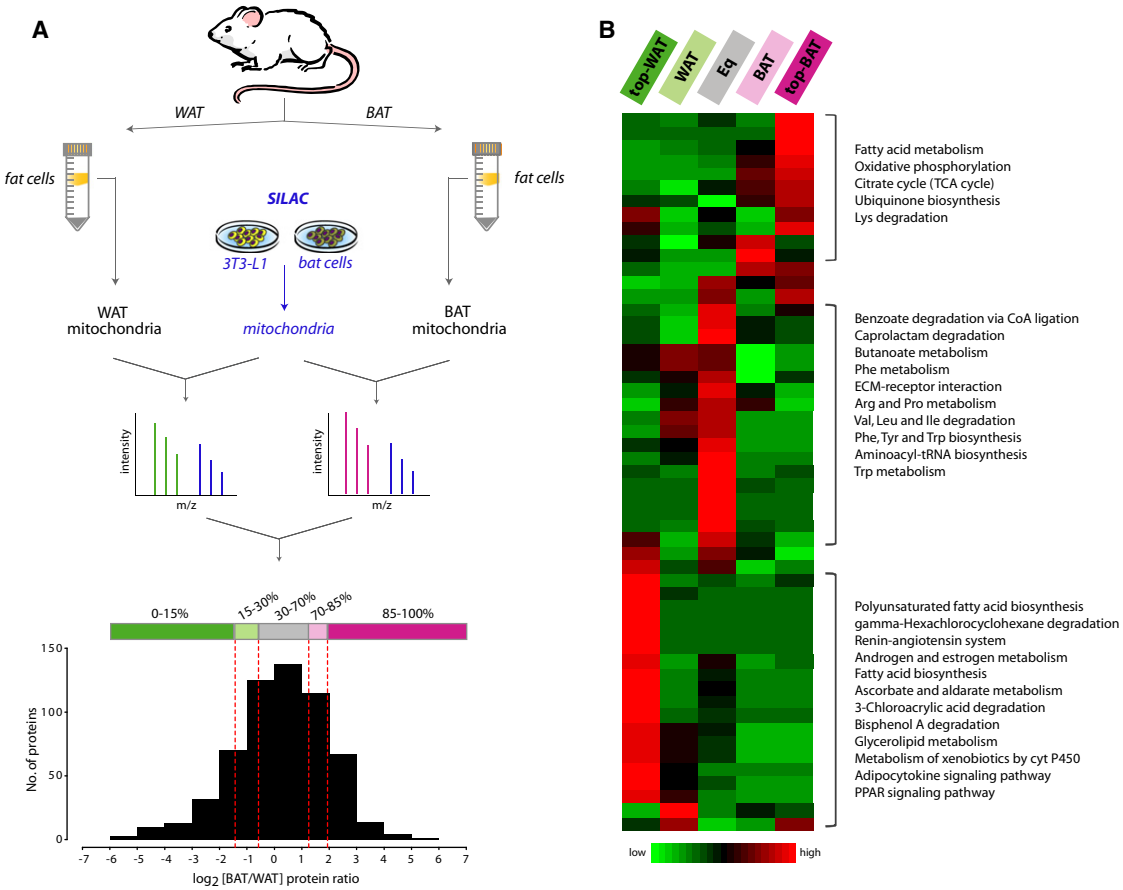

Figure 3. Quantitative Protein Analysis of Brown versus White Fat Cell Mitochondria

(A) Mitochondria are enriched from floating fat cells isolated by disaggregation of white and brown fat depots. Mitochondria from SILAC-labeled adipocyte cell lines serve as internal references for MS quantitation of tissue peptides. The protein ratio distribution is divided in five color-coded percentiles (top-BAT, BAT, Equal, WAT, and top-WAT) based on relative BAT versus WAT enrichment.

(B) Heat map of overrepresented pathways ($p < 0.05$) in each of the five categories.

and MitoCarta adipose tissue compendium (mapped to 831 IPI identifiers) (Pagliarini et al., 2008). Of the 68% unambiguously assigned proteins in MitoCarta, we mapped 78%, and we provide 771 novel mitochondrial or mitochondrial associated proteins in isolated fat cells (Figure 2B). GO annotation relies on large-scale experiments, many of which are not quantitative, and the database is not tissue specific. Accordingly, we mapped 46% of GO-annotated mitochondrial proteins.

Quantitative Analysis of BAT and WAT Mitochondrial Proteomes

We next wished to accurately quantify the WAT against the BAT mitochondrial proteomes in vivo. We first prepared a SILAC internal standard consisting of combined crude mitochondrial fractions from heavy metabolically labeled 3T3-L1 and a cell line of brown adipocytes. Then homogeneous populations of lipid-filled adipocytes were isolated from brown and white adipose tissues and subfractionated to enrich mitochondria. Mitochondrial fractions were combined with the internal standards, and proteins were analyzed by high-resolution MS (Figure 3A). In total, 2434 proteins were confidently identified with a false positive rate of less than 1% and average absolute mass accuracy of 1 ppm across all measured peptides. We then extracted 1045 proteins that were present in our consolidated mitochondrial fat cell proteome derived above. The relative in vivo abundances of mitochondrial proteins in BAT versus WAT were then determined as the ratio of ratios of internal standard to tissue for both BAT and WAT. Applying further stringent requirements for the consistency of quantitation, we obtained a core of 684 proteins reproducibly quantified across replicate experiments (Table S4).

Global Functional Assessment of BAT and WAT Mitochondria

The proteins quantified between BAT and WAT were then categorized and color coded in five quantiles: top-WAT (dark green), WAT (light green), equal (gray), BAT (light red), and top-BAT (dark red). Each of these quantiles was analyzed for KEGG overrepresentation of pathways ("proteomic phenotyping" [Pan et al., 2009]) to obtain functional insights into the differences between BAT and WAT mitochondria directly from quantitative proteomic data. Hierarchical clustering then yielded a heat map of the overrepresented pathways and functions (Figure 3B). This resulted in a system-wide functional map that highlighted clearly distinct metabolic signatures of mitochondria (Table S5).

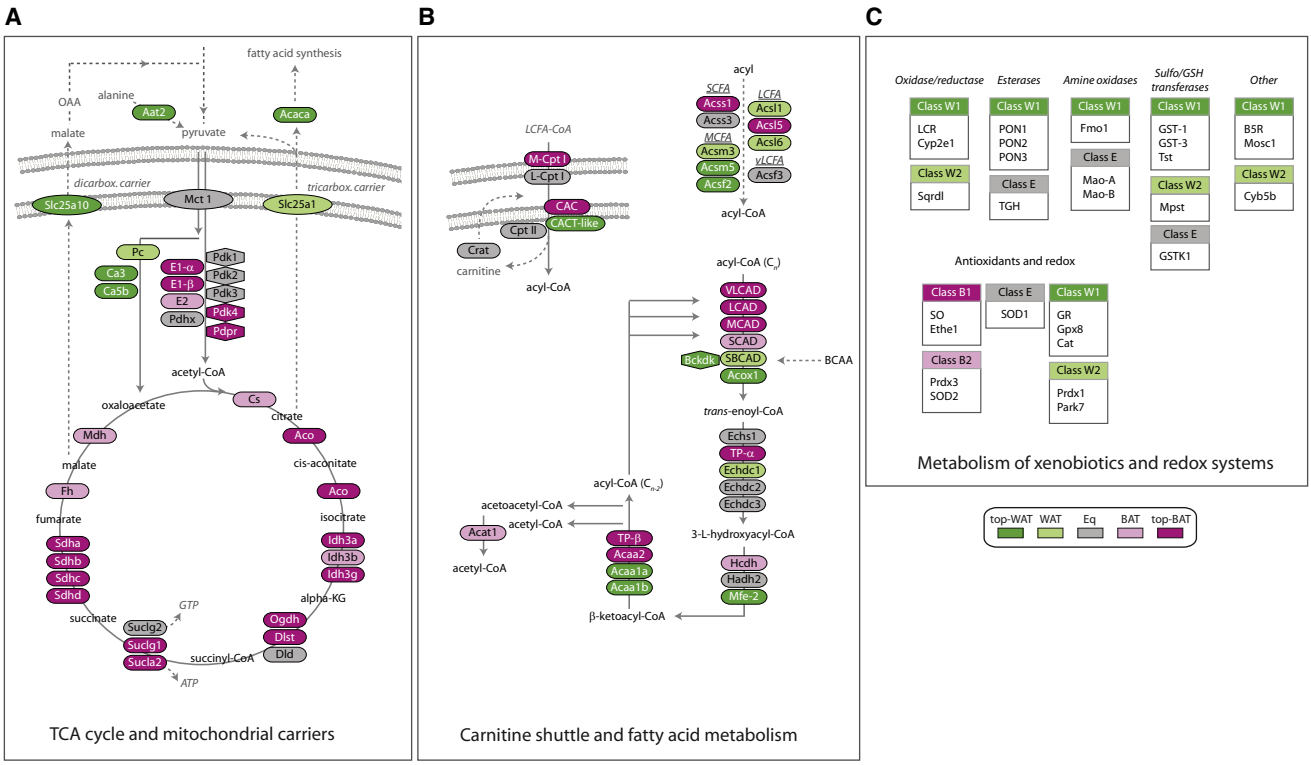

Figure 4. Relative Activity of Mitochondrial Pathways in BAT versus WAT

The colors represent relative enrichment of proteins in BAT versus WAT (magenta, top-BAT; pink, BAT; gray, equal; green, WAT; dark green, top-WAT).

(A) Pyruvate dehydrogenase and TCA cycle.

(B) Lipid metabolic pathways showing different ACS isoforms, the carnitine shuttle, and mitochondria-localized enzymes involved in the oxidation of fatty acids.

(C) Enzymes involved in the transformation of endogenous substrates, detoxification from xenobiotics, and ROS divided in functional categories.

Functions such as oxidative phosphorylation, fatty acid metabolism, and citrate cycle were predominant in brown fat. In contrast, white fat mitochondria were characterized by anabolic functions such as glycerolipid and fatty acid biosynthesis, and surprisingly by several pathways ascribed to biotransformation of endo- or xenobiotics (see below). Importantly, this overall map of functions is directly linked to quantitative ratios of pathways, protein complexes, individual subunits, and isoforms.

Tissue Specificity of Oxidative Phosphorylation and TCA Cycle

Our SILAC-based proteome comparison mapped and quantified subunits of the oxidative phosphorylation chain with almost complete coverage (Table S4). Relative fold enrichments were generally consistent among subunits within the same complex—this is illustrated by the subunits α and β of ATP-synthase, which forms stoichiometric $\alpha_3\beta_3$ subcomplexes, and by succinate dehydrogenase, which forms a heterotetrameric structure (Table S6). While members of Complex I-IV were more highly expressed in BAT, Complex V (ATP-synthase) was present at higher relative level in WAT (average of 1.6-fold). In BAT mitochondria, Complex V is bypassed for heat generation; therefore our ratios for members of the respiratory chain directly reflect the major physiological function of BAT.

The TCA cycle and related enzymes were also clearly predominant in BAT (Figure 4A). Interestingly, we found different fold changes in the expression of the β subunits of succinyl-CoA synthetase (SCS), a heterodimer composed of a single α subunit and two different β subunits that determine nucleotide specificity (Lambeth et al., 2004). The GDP-forming subunit (G-SCS-β) had equal levels in both tissues, whereas the ADP-forming subunit (A-SCS-β) was 7-fold more highly expressed in BAT. This may indicate differences in relative utilization of GDP and ADP in the two fat tissues.

The pyruvate dehydrogenase complex (PDC) also showed tissue-specific regulation. One of the inhibiting kinases, PDK4, was uniquely expressed in BAT as judged by MS, whereas the other three isoforms (PDK 1-2-3) were expressed in both tissues at similar levels (Table 1). Additionally, the PDPr subunit of PDC phosphatase was highly enriched in BAT. These data suggest that PDC activity has a specific and more complex regulation in BAT cells compared to WAT cells.

Conversely, lipogenic and gluconeogenic routes involving the TCA cycle were clearly predominant in WAT as highlighted by enrichment of pyruvate carboxylase (PC), di- and tricarboxylate transporters (Slc25a1 and Slc25a10), acetyl-CoA carboxylase (Acaca), and alanine aminotransferase (Aat2) (Figure 4A). We also observed about 20-fold enrichment of carbonic anhydrase CA V and CA III. Although the role of these enzymes in adipose tissue is still unclear, a possible relation of CA V to de novo lipogenesis has been suggested and would be consistent with our data (Hazen et al., 1996).

Table 1. Highly Characterizing Mitochondrial Proteins in Brown versus White Fat Cells

Description	Gene	Fold Enrichment
Top-BAT Proteins		In BAT
Acetyl-CoA synthetase 2-like	Acss1	Only detected in BAT
Pyruvate dehydrogenase kinase 4	Pdk4	Only detected in BAT
Chaperone-ABC1-like	Cabc1	65
CPT	Cpt1b	51
Uncoupling protein-1	Ucp1	25
3-ketoacyl-CoA thiolase	Acaa2	25
LETM1 domain-containing protein 1	Letmd1	19
Uncharacterized protein C18orf19 homolog (ID Q8BGY7)		18
Protein HRPAP20	Hrpap20	14
2310061I04Rik protein	2310061I04Rik	14
Solute carrier family 25 member 42	Slc25a42	11
Top-WAT Proteins		In WAT
MOSC domain-containing protein 1	Mosc1	Only detected in WAT
Acyl-coenzyme A synthetase ACSM5	Acsm5	Only detected in WAT
Nonspecific lipid-transfer protein	Scp2	66
Casein kinase II subunit α	Csnk2a1	54
Alanine aminotransferase 2	Aat2	21
Carbonic anhydrase 3	Ca3	20
Carbonic anhydrase 5B	Ca5b	20
17-β-hydroxysteroid dehydrogenase 4	Mfe-2	17
Mitochondrial dicarboxylate carrier	Slc25a10	15
1-acyl-sn-glycerol-3-phosphate acyltransferase	Agpat3	12
Mitochondrial fission 1 protein	Fis1	12

In the table are proteins that showed highest relative protein enrichments in BAT versus WAT as determined by MS.

Specific Isoforms Determine Fatty Acid Metabolism

Our data show that mitochondria employ specific isoforms to carry out degradation and biosynthesis of fatty acids (Figure 4B). Of particular interest is the predominance of certain acyl-CoA synthetases (ACS) isoforms, crucial enzymes that activate fatty acids to thioesters. Due to the diverse chemical properties of fatty acids, higher organisms contain multiple enzymes with ACS activity (Watkins et al., 2007). Therefore, determining the relative abundance of ACS is fundamental to understand what substrates are preferentially utilized in different tissues. Among the short-chain ACSs, ACSS1 was BAT unique and very abundant in this tissue (Table 1). The function of ACSS1 is to preferentially activate acetate which is then oxidized under ketogenic conditions such as starvation (Fujino et al., 2001; Sakakibara et al., 2009). Conversely, ACSM3, ACSM5, and ACSF2 (medium-chain specificity) were all consistently predominant in WAT. Long-chain-specific isoforms were also distributed in a tissue-dependent manner, with ACSL1, ACSL6, and ACSF3 higher in WAT, whereas ACSL5 was higher in BAT. mRNA expression profiles of ACS in chow-fed rats showed that ACSL5 is clearly predominant in brown fat at the transcript level (Mashek et al., 2006a). Once activated, long-chain fatty acids (LCFAs) require carnitine palmitoyltransferase (CPT) to be gated into mitochondria, and here we found that the CPT1-M isoform was more than 50-fold enriched in BAT (Table 1), whereas CTP1-L had similar levels. Taken together, these findings imply that BAT preferentially activates LCFA and has much lower medium-chain fatty acid activation as compared to WAT. However, the relative upregulation of ACSL5 may also partition fatty acids toward TAG synthesis rather than toward mitochondrial β oxidation (Mashek et al., 2006b).

Long-, medium-, and short-chain acyl-CoA dehydrogenases (Acad), enzymes that catalyze the first step of the β oxidation pathway, were all predominant in BAT, whereas the short/branched chain Acad (SBCAD) was higher in WAT. Accordingly, the SBCAD kinase (Bckdk) was very high in white fat, implying critical control of branched-chain amino acid (BCAA) utilization in this tissue. Likewise, we found tissue-specific expression of several other enzymes that catalyze different steps of the fatty acid oxidation pathways (Figure 4B). Interestingly, the 25-fold enrichment of 3-ketoacyl-CoA thiolase (Acaa2) in BAT is equal to that of UCP1.

Traditionally, enzymes that catalyze the biosynthetic pathway that form TAG and glycerophospholipids have been thought to be exclusively cytoplasmic. However, recent reports have shown that GPAT1, GPAT2, and DGAT2, enzymes that catalyze the first and final steps of the pathway, are located or associated with the outer mitochondrial membrane (Gonzalez-Baro et al., 2007; Stone et al., 2009). It has also been suggested that mitochondrial GPAT might compete with CPT1 for the same LCFA substrates. In our study, we found the mitochondrial isoform Gpam, AGPAT2, AGPAT3, DGAT1, Agk, and Acp6 specifically enriched in white mitochondrial fractions (but also expressed in brown mitochondria), although the AGPAT isoforms are

traditionally associated with the endoplasmic reticulum. Taken together, these findings raise the possibility that a pathway with TAG biosynthetic activity is closely associated with adipocyte mitochondria.

White Fat Has a Prominent Detoxification Function

A large class of enzymes whose activity is related to the biotransformation of drugs, dietary substances, and other synthetic and environmental agents is enriched in WAT mitochondria (Figure 4C, Table S4). This class of proteins has so far not been investigated with respect to WAT function. These proteins are related to both phase I and phase II biotransformation reactions and have different substrate specificities. Enzymes with phase I activity included P450 monooxygenase (CypIIE1); amine oxidases such as FMO1, MAO-A, and MAO-B; carbonyl reductase (LCR); quinone oxidoreductase (Sqrdl); and esterases such as triacylglycerol hydrolase (TGH). Among phase II enzymes, we identified rhodanese (Tst) and several glutathione S-transferases (GST-1, GST-3, and GSTK1-1).

WAT also predominantly expressed several isoforms of the aldehyde dehydrogenase superfamily. We conclude that white fat cells, similarly to hepatocytes, have a prominent role in the transformation of xenobiotics and endogenous molecules and that mitochondria also take part into these functions.

The only detoxification proteins that were higher in BAT mitochondria were ETHE1 and sulfite oxidase (SO), which were both 6-fold enriched. Recently ETHE1 was shown to have sulfur dioxygenase activity (Tiranti et al., 2009). High levels of ETHE1 and SO might suggest that detoxification from sulfur compounds such as H_2S, an inhibitor of cytochrome oxidase, is crucial in tissues that rely on high aerobic respiration rates.

BAT Mitochondria Are More Similar to Muscle Than to WAT Mitochondria

In previous work we had examined mitochondrial proteomes in rat skeletal muscle, heart, and liver and established a strong tissue-dependent expression of several proteins (Forner et al., 2006b). These tissue-specific proteins were mapped to BAT and WAT mitochondria. WAT mitochondrial proteins had a relatively large overlap with the liver mitochondria, whereas the BAT-enriched proteins clearly overlapped with proteins from muscle mitochondria (Figure S1). In particular, both tissues were characterized by high pyruvate and fatty acid oxidation activities. Furthermore, Cabc1 and Pdk4 were among the most abundant enzymes in both BAT and skeletal muscle mitochondria. WAT mitochondria exhibited some functional overlap with liver mitochondria in proteins related to metabolism of fatty acids and detoxification functions.

To establish at a different level of gene expression which tissues the brown and white fat cell mitochondria were most related to, we obtained mRNA levels across several organ and tissues from GNF mouse atlas version 3 (Lattin et al., 2008). Two-way hierarchical clustering revealed clear patterns of tissue-specific expression (Figure S2). Brain tissues have a distinct expression profile and cluster separately from the other investigated tissues. Among the nonbrain tissues, BAT again aligned with muscle tissue, and strikingly 165 genes were highly and preferentially expressed in muscle tissues and BAT, including Complex I, Carnitine palmitoyltransferase (Cpt1b), Chaperone-ABC1-like (Cabc1), Pyruvate dehydrogenase kinase (Pdk4), Superoxide dismutase (Sod2), and Peroxiredoxin (Prdx3) (Table S7). WAT did not cluster with BAT or muscle but was instead more closely related to other organs. Interestingly, some uncharacterized genes (such as Brp44, Letmd1, and the uncharacterized protein C18orf19 homolog) are expressed at high levels in BAT and muscle, but not WAT. Thus, they may be involved in mitochondrial oxidative metabolism, which is very high in these tissues.

BAT and muscle have the capacity to perform adaptive thermogenesis, and recently it has been shown that brown fat cells and muscle cells, but not white fat cells, derive from the same lineage (Atit et al., 2006; Seale et al., 2008; Timmons et al., 2007). These findings provide a developmental explanation of our observations at the mitochondrial transcriptome and proteome levels.

BAT Mitochondrial Remodeling upon Cold Exposure

To functionally characterize the BAT mitochondrial proteome, we chose to study its remodeling upon acute and chronic cold exposure. Cold exposure immediately activates nonshivering thermogenesis (NST) mediated by the dense sympathetic innervations of brown adipose tissue. Chronic cold exposure with sustained sympathetic stimulation of brown adipose tissue results in a very well-characterized recruitment process involving proliferation and differentiation of brown preadipocytes, tissue growth, mitochondrial biogenesis, and upregulation of Ucp1 gene expression (Klaus et al., 1991; Klingenspor, 2003).

We isolated interscapular brown fat depots from cold-exposed chow-fed mice (4°C) after acute (4 days) and chronic (24 days) exposure and extracted crude mitochondrial fractions. During this time, both BAT depot mass and extracted mitochondrial proteins increased significantly (Figure 5A). To distinguish true mitochondrial proteins from the background, we employed the mitochondrial proteome determined above. We applied SILAC-based quantitative proteomics by mixing heavy labeled mitochondria from a brown fat cell line into the crude tissue mitochondrial preparation. This labeled internal standard then allowed analysis of quantitative proteomic changes across the time course experiment. Equal amounts of mitochondrial tissue fractions were used; therefore our analysis compares mitochondria before and after cold exposure on a "per mitochondria" basis—over and above the increase in the number of mitochondria.

Our time course experiment resulted in a large, quantified proteome across the three conditions (Table S8). As highlighted by cluster and pathway analysis, cold exposure induced preferential upregulation of pathways that were BAT enriched in the above BAT versus WAT comparison, such as oxidative phosphorylation, ubiquinone biosynthesis, and TCA cycle. However, we also observed upregulated levels of enzymes involved in the synthesis of glycerophospholipids (Figure S3A). Conversely, functions such as xenobiotic metabolism and cell communication were downregulated by cold exposure (Figure S3B).

The key adaptation to cold exposure in BAT mitochondria was the synthesis and assembly of the complexes of the respiratory chain, and in particular most subunits of Complex I. However, upregulation was not uniform for all subunits of each complex, which indicates changes in complex composition and suggests

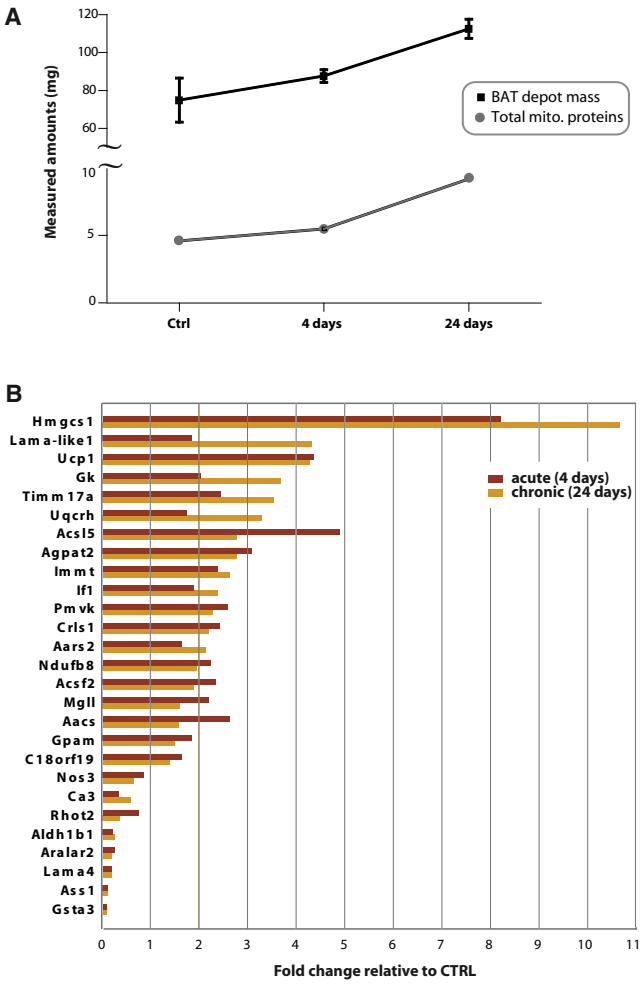

Figure 5. BAT Modulation upon Cold Exposure

(A) Wet weight of brown adipose tissue (mg); values are means ± SEM (n = 4–8). Mitochondrial protein amounts in the BAT depots (expressed in mg) were determined by the Biuret assay.

(B) Proteins that showed at least 2-fold up- or downregulation upon cold exposure are shown in the bar graph. Protein fold changes in the acute and chronic cold exposure phases are determined with respect to the control group (mice kept at room temperature).

critical and rate-limiting roles for specific subunits. Other studies have already reported that the assembly of multisubunit complexes in the mitochondrial membrane may be limited by the abundance of one or few subunits (Kramarova et al., 2008).

Levels of UCP1 were 4-fold increased, which made it one of the most highly regulated proteins, emphasizing its essential role in NST (Figure S4 and Figure 5B). We observed a 2-fold increase of the ATPase inhibitor (If1), which usually inhibits the switch of ATP synthase to ATPase activity in the presence of uncoupling agents (Schwerzmann and Pedersen, 1986). If1 upregulation may serve to downregulate ATP hydrolysis in brown fat mitochondria with an active thermogenic proton leak. Levels of the ATP synthase subunits were unchanged.

Fatty acid metabolism appeared modulated in an isoform-specific basis during cold adaption. In particular, the ACS isoform ACSL5 was increased approximately 3- and 5-fold upon acute and chronic cold exposure, respectively, whereas ACSF2, an ACS isoform predominant in WAT, increased only 2-fold (Figure 5B). We initially expected marked upregulation of fatty acid oxidative activity in general because of increased energy demand. However, levels of enzymes of the mitochondrial β oxidation pathway were largely unchanged, suggesting that mitochondrial biogenesis might be sufficient to meet acyl-CoA requirements during NST. CPT1-M (the BAT-specific isoforms of CPT1) was increased—but only about 1.5-fold, whereas the CPT1-L isoform (equally distributed in BAT and WAT) was slightly downregulated. The only clearly upregulated lipolytic enzymes were monoglyceride lipase (2-fold) and phospholipase B-like 1 (2- to 4-fold, indicated as Mg II and LAMA-like 1 in Figure 5B).

Mitochondrial biogenesis was reflected by upregulation of hydroxymethylglutaryl-CoA synthase (Hmgcs1), phosphomevalonate kinase (Pmvk), and cardiolipin synthase (Crls1), cytosolic enzymes present in our crude preparations that synthesize mitochondrial membrane lipids cholesterol and cardiolipin. Furthermore, distinct upregulation of Agpat2 and glycerol kinase (GK) and slight upregulation of Gpam indicate enhanced TAG synthesis. Increased activity of the mitochondrial GPAT isoform has previously been observed in BAT after 12 days of cold acclimation (Darnley et al., 1988). Furthermore, previous studies also reported activation of glyceroneogenesis (Moura et al., 2005) and of lipogenic routes (Jakus et al., 2008; Yu et al., 2002) in cold-challenged animals. Taken together, our findings show that the TAG and phospholipid pathway are activated during cold adaption, correlating with the increase in brown fat depots and mitochondria.

DISCUSSION

Here we have described a systematic analysis of mitochondrial functions in brown and white adipocytes based on accurate determination of in vivo protein ratios using mitochondria from SILAC-labeled cell lines as internal standards. Protein identifications were done at very high resolution, confidence, and sensitivity.

The quantitative approach that we have described to assign mitochondrial protein localization circumvents long-standing experimental limitation. We performed a localization experiment that enabled us to efficiently distinguish between true mitochondrial proteins and background proteins based exclusively on the criterion of protein enrichment across different samples. This method is generally applicable to any structure or organelle that can be biochemically enriched. For example, in the field of mitochondrial proteomics it could also be applied to predict the submitochondrial localization of mitochondria-localized proteins. Mapping the tissue-specific mitochondrial proteome in great depth, as described here, is a precondition to study its functions in a system-wide, unbiased way.

High-accuracy quantitative proteomics resulted in protein-by-protein expression differences, which we employed for a systematic molecular-level understanding of mitochondrial functions on a cell-specific basis. Notably, our analysis revealed that, in addition to different expression levels, mitochondria from brown and white adipocytes employ different protein isoforms to a substantial degree. This was easily mapped by MS through differentiating peptides and is fundamental to understanding

what substrates are preferentially utilized and how energy management is performed in brown and white fat cells.

In particular, relatively high levels of ACSF5 and ACSS1 in brown fat mitochondria suggest that LCFAs and acetate are major metabolic fuels in BAT. Conversely, the predominance of medium-chain ACS in white fat mitochondria implies that these substrates are much more relevant in WAT.

Based on gene-level and protein-level cluster analyses, we discovered a close relationship between the metabolic features of BAT and muscle mitochondria. This finding is of interest in respect to recent reports on a common myoblast-like ''adipomyoblast'' progenitor of brown adipocytes and muscle cells (Atit et al., 2006; Seale et al., 2008; Timmons et al., 2007). Our data demonstrate that this common developmental origin can be detected on the level of the mitochondrial proteome when comparing fully differentiated brown adipose tissue and skeletal muscle. We propose that the metabolic properties of muscle mitochondria represented the essential prerequisites for the evolution of thermogenic mitochondria in brown adipocytes.

Conversely, mitochondria of white adipocytes support lipogenic functions. Interestingly, we found predominance in WAT of enzymes involved in TAG synthesis. Localization of GPAT1 and GAPT2 at the outer mitochondrial membrane has already been reported (Wendel et al., 2008). Furthermore, our work reveals the presence of several enzymes with diverse substrate specificities involved in detoxification from xenobiotics and in degradation of endogenous molecules. This system appears negligible in BAT. Although xenobiotics are usually metabolized in the liver (Eloranta et al., 2005), it is known that several lipophilic compounds accumulate in extrahepatic tissues including adipocytes. Thus this detoxification mechanism adds a protective role to the functions of this tissue.

For possible clinical relevance of BAT and strategies aimed at the reduction of excess fat accumulation by increasing energy expenditure, our results provide a detailed map of metabolic differences between the two fat cell types that are appreciably dissimilar.

We also discovered BAT-specific proteins that are regulated by cold exposure. By design, our study determined all changes on a ''per mitochondrium'' basis. Our results show that in addition to upregulation of mitochondrial mass, respiratory potential was drastically increased in cold exposed mice as judged by additional upregulation of UCP1 and of Complex I. Furthermore, our results suggest specific, rate-limiting functions of specific respiratory complex subunits because they were selectively upregulated. Interestingly, we also observed upregulation of proteins that are more predominant in WAT (e.g., Agpat2, Acsf2, and Gpam), implying a net increase of TAG biosynthesis during adaptive NST.

In summary, we have determined the mitochondrial proteome in adipose cells in great depth and with high accuracy. Quantitation of metabolic enzymes or of the members of any pathways in different cell types should become a powerful method to derive functional data from proteomic comparisons. Clarification of the proteomic characteristics of BAT and WAT mitochondria is an important step in obtaining a better molecular-level understanding of physiological processes in these tissues and should provide a resource aiding in the design of therapeutic interventions for metabolic diseases.

EXPERIMENTAL PROCEDURES

Additional methods are available in the Supplemental Experimental Procedures.

SILAC Internal Standards

3T3-L1 and a cell line of brown preadipocytes (kindly provided by R.C. Kahn) were subcultured (four passages) and differentiated in SILAC-DMEM supplemented with 10% 10 kDa-dialyzed fetal bovine serum (GIBCO) and antibiotics in 5% CO_2 at 37°C. The SILAC-DMEM was custom made and was deficient for L-Arg and L-Lys (Invitrogen). L-arginine-10 ($^{13}C_6$,-$^{15}N_4$-Arg) and L-lysine-8 ($^{13}C_6$,-$^{15}N_2$-Lys) (Sigma Aldrich, Isotec) were supplemented to the medium to final concentrations of 25.2 mg/l and 48.62 mg/l, respectively. 3T3-L1 preadipocytes were grown and differentiated as described previously (Kratchmarova et al., 2002). Brown preadipocytes were differentiated as described (Fasshauer et al., 2001). Cells were harvested with trypsin (GIBCO), diluted with DMEM supplemented with protease inhibitors (Roche) and centrifuged at 1000 × g for 10 min. Cells were then resuspended with 250 mM sucrose, 10 mM HEPES (pH 7.4), 0.1 mM EGTA supplemented with protease inhibitors (Roche) and washed twice. The suspension was homogenized on a 7 ml Dounce homogenizer and centrifuged at 800 × g for 10 min at 4°C to isolate the crude nuclear fraction (Nuc). The supernatant was further centrifuged at 10,000 × g for 10 min at 4°C, and the crude mitochondrial fraction was purified on a 30% Percoll self-forming gradient.

Equal amounts of brown and white SILAC mitochondria were mixed 1:1 based on the protein amount and served as the internal standard.

The postmitochondrial fraction (PMF) was obtained as the supernatant after the centrifugation at 10,000 × g. PMF proteins were concentrated by centrifugation with 5,000 MWCO membranes (Millipore).

Isolation and Subcellular Fractionation of Fat Cells

Interscapular brown adipose tissue and epididymal white adipose tissue were excised from chow-fed groups of 5 C57BL/6 mice (5 to 10 weeks old). Fat pads were immersed in HBSS, cleaned of connective tissue under a binocular microscope, minced, and digested with 1 mg/ml collagenase A (Roche) at 37°C for 30 min. After digestion, the slurry was passed through 250 μm mesh opening fiber material (Sefar) and centrifuged at 500 × g for 1 min. The floating adipocytes were removed with a plastic pipette and centrifuged three additional times in HBSS. No visible stromal vascular fraction was present after the fourth centrifugation. Floating adipocytes were homogenized in ice using a 10 μm clearance precooled cell homogenizer (Isobiotec). Membrane disruption was checked with trypan blue staining. The tissue homogenate was centrifuged twice at 800 × g for 10 min at 4°C. The supernatant was centrifuged at 10,000 × g for 10 min at 4°C. The crude mitochondrial pellet was resuspended in 250 mM sucrose, 10 mM HEPES (pH 7.4), 0.1 mM EGTA supplemented with protease inhibitors (Roche). The suspension was further centrifuged at 7,000 × g for 10 min at 4°C and purified with the protease treatment as described (Forner et al., 2006a). For quantitative proteomic analyses, mitochondria from the brown and from the white adipose tissues were each mixed 1:1 with the internal standard (see the Supplemental Experimental Procedures) based on protein amount (Bradford). The experiment was performed in triplicate.

For the localization study, mitochondria (Mito) from the brown and from the white adipose tissues were mixed 1:1 with PMF and Nuc fractions isolated from the SILAC-labeled brown adipocytes or 3T3-L1 respectively (described in the Supplemental Experimental Procedures).

Bioinformatics of Mitochondrial Localization

Bayesian inference methodology was used to assign localization probabilities for organellar proteins in white and brown adipocytes. Mitochondrial protein enrichment (*Mito*) was determined against (1) PMF and (2) Nuc.

(1) For mitochondria + PMF, we used the statistical method of finite mixture modeling to model the abundances of the $\log_2(\frac{PMF}{Mito})$ratios based on the assumption that the "*Mito*" and "*PMF*" protein ratios originate from two different Gaussian distributions $f(x;\mu_{Mito},\sigma_{Mito})$and $f(x;\mu_{PMF},\sigma_{PMF})$, respectively. The distributions were estimated by EM algorithm using the SILAC ratios for all the proteins identified in the experiment. P_{Mito} and P_{PMF}, probabilities of

membership to mitochondrial (C_{Mito}) and PMF (C_{PMF}) classes, were calculated for each protein from the protein ratio $x = \log_2(\frac{PMF}{Mito})$ by the following equations:

$$P_{Mito} = P(C_{Mito}|Ratio = x) = \frac{P(Ratio = x|C_{Mito}) * P(C_{Mito})}{P(Ratio = x|C_{Mito}) * P(C_{Mito}) + P(Ratio = x|C_{PMF}) * P(C_{PMF})}$$

And

$$P_{PMF} = P(C_{PMF}|Ratio = x) = \frac{P(Ratio = x|C_{PMF}) * P(C_{PMF})}{P(Ratio = x|C_{Mito}) * P(C_{Mito}) + P(Ratio = x|C_{PMF}) * P(C_{PMF})}$$

where,

$P(Ratio = x|C_{Mito}) = f(x; \mu_{Mito}, \sigma_{Mito})$

$P(Ratio = x|C_{PMF}) = f(x; \mu_{PMF}, \sigma_{PMF})$

(2) Mitochondria + nuclei was as in case 1, with the $\log_2(\frac{Nuc}{Mito})$ratios as the input. The analysis was done using "MCLUST" version 3 package in R (Fraley and Raftery, 2002). For each of (1) and (2), proteins were assigned to organellar categories based on their localization probability values.

(1) Based on the P_{Mito} *and* P_{PMF} membership probabilities for each protein, we categorized the proteins in three categories: (1) MITO, if ($P_{Mito} >= 0.75$); (2) BORDER, if ([$P_{Mito} < 0.75$] and [$P_{PMF} < 0.75$]); and (3) non-MITO, if ($P_{PMF} >= 0.75$).

(2) Based on the P_{Mito} *and* P_{Nuc} membership probabilities for each protein, we categorized the proteins in three categories: (1) MITO, if ($P_{Mito} >= 0.75$); (2) BORDER, if ([$P_{Mito} < 0.75$] and [$P_{Nuc} < 0.75$]); and (3) non-MITO, if ($P_{Nuc} >= 0.75$).

The accuracy of the localization assignment was defined with respect to known GO mitochondrial annotations (GO:0005739) available for IPI v3.37. To evaluate the percentage of true positive and false negative mitochondrial proteins assigned by our approach, we define two metrics, namely true localization percentage (TLP) and false localization percentage (FLP), as defined below:

$$TLP = \frac{(\text{Proteins in MITO class}) \text{ AND } (\text{Annotated as Mitochondrial } (GO{:}0005739))}{\text{All Proteins Annotated as Mitochondrial}(GO{:}0005739) \text{ in dataset}} * 100$$

$$FLP = \frac{(\text{Proteins in Non-MITO class}) \text{ AND } (\text{Annotated as Mitochondrial } (GO{:}0005739))}{\text{All Proteins Annotated as Mitochondrial}(GO{:}0005739) \text{ in dataset}} * 100$$

Mass Spectrometry and Data Analysis

Protein samples were separated on 4%–12% acrylamide gels (Invitrogen). Each gel lane was divided in ten slices, and peptides were extracted by in-gel digestion with trypsin as described (Forner et al., 2006b). Peptides were desalted and concentrated on C_{18} Stage Tips as described (Rappsilber et al., 2003) and analyzed by LC-MS/MS on a LTQ-Orbitrap mass spectrometer (Thermo Fischer Scientific) connected to an Agilent 1200 nanoflow HPLC system via a nanoelectrospray source (Proxeon Biosystems). MS full scans were acquired in the orbitrap analyzer in using internal lock mass recalibration in real time. MS full scans were acquired in two different m/z ranges (350–1000 and 1000–1800). Tandem mass spectra of the six most intense ions of the lower mass range and subsequently of the four most intense ions of the higher mass range were simultaneously recorded in the linear ion trap. Peptides were identified from MS/MS spectra by searching them against the IPI mouse database (v3.37) using the Mascot search algorithm (http://www.matrixscience.com/) and SILAC pairs were detected and quantified using the MaxQuant algorithms (Cox and Mann, 2008). Requirements for protein identification were at least two nonoverlapping peptide sequences, one of which had to be unique to the isoform, and a false positive rate of less than 1%, determined from reverse database searching.

Mitoproteomics upon Cold Exposure

C57BL/6 mice (3 months old) were kept in a 12:12 hr light:dark photoperiod and fed a standard chow diet (Ssniff) with water ad libitum. Mouse experiments were conducted in accordance with the German animal welfare law. Mice were divided in three groups of eight mice each. Two groups were kept in a climate chamber at 4°C for either 4 days or 24 days, respectively; the control group was kept at room temperature. At the time of the experiment, the mice were approximately all of the same age. Brown fat pads were isolated from the interscapular region and minced free of connective tissue and visible white fat, and lipid-filled adipocytes isolated as described above. The crude mitochondrial fraction was isolated as described above. Of SILAC-labeled mitochondria, 100 μg isolated from a cell line of brown adipocytes (kindly provided by B. Spiegelman [Uldry et al., 2006]) were spiked 1:1 with BAT mitochondria based on protein amount (Bradford and Biuret).

Proteins were in-solution digested with Lys-C followed by trypsin. Peptides were separated in 12 fractions by isoelectric focusing on a 3100 Offgel fractionator (Agilent Technologies) using 13 cm Immobiline DryStrip in the pH range 3–10 (GE Healthcare) (Hubner et al., 2008). Peptides were desalted on StageTips before mass spectrometric analysis. MS was performed essentially as described above (see the Supplemental Experimental Procedures).

SUPPLEMENTAL DATA

Supplemental Data include Supplemental Results, Supplemental Experimental Procedures, Supplemental References, eight tables, and four figures and can be found with this article online at http://www.cell.com/cell-metabolism/supplemental/S1550-4131(09)00264-2.

ACKNOWLEDGMENTS

We thank Korbinian Mayr and Sonja Krüger for excellent technical assistance, and Andisheh Abedini and Mara Monetti for critical reading of the manuscript. This work was supported by the Diabetes Genome Anatomy Project (DGAP, National Institutes of Health grants DK60837) and by Interaction Proteome, a Sixth Framework Program of the European Union.

Received: April 22, 2009
Revised: July 24, 2009
Accepted: August 28, 2009
Published: October 6, 2009

REFERENCES

Andersen, J.S., and Mann, M. (2006). Organellar proteomics: turning inventories into insights. EMBO Rep. *7*, 874–879.

Ashburner, M., Ball, C.A., Blake, J.A., Botstein, D., Butler, H., Cherry, J.M., Davis, A.P., Dolinski, K., Dwight, S.S., Eppig, J.T., et al. (2000). Gene Ontology: tool for the unification of biology. The Gene Ontology Consortium. Nat. Genet. *25*, 25–29.

Atit, R., Sgaier, S.K., Mohamed, O.A., Taketo, M.M., Dufort, D., Joyner, A.L., Niswander, L., and Conlon, R.A. (2006). Beta-catenin activation is necessary and sufficient to specify the dorsal dermal fate in the mouse. Dev. Biol. *296*, 164–176.

Cinti, S. (2005). The adipose organ. Prostaglandins Leukot. Essent. Fatty Acids *73*, 9–15.

Cox, J., and Mann, M. (2008). MaxQuant enables high peptide identification rates, individualized p.p.b.-range mass accuracies and proteome-wide protein quantification. Nat. Biotechnol. *26*, 1367–1372.

Crunkhorn, S., and Patti, M.E. (2008). Links between thyroid hormone action, oxidative metabolism, and diabetes risk? Thyroid *18*, 227–237.

Darnley, A.C., Carpenter, C.A., and Saggerson, E.D. (1988). Changes in activities of some enzymes of glycerolipid synthesis in brown adipose tissue of cold-acclimated rats. Biochem. J. *253*, 351–355.

Dempster, A.P., Laird, N.M., and Rubin, D.B. (1977). Maximum likelihood from incomplete data via the EM algorithm. J. R. Stat. Soc. [Ser A] *39*, 1–38.

Eloranta, J.J., Meier, P.J., and Kullak-Ublick, G.A. (2005). Coordinate transcriptional regulation of transport and metabolism. Methods Enzymol. *400*, 511–530.

Fasshauer, M., Klein, J., Kriauciunas, K.M., Ueki, K., Benito, M., and Kahn, C.R. (2001). Essential role of insulin receptor substrate 1 in differentiation of brown adipocytes. Mol. Cell Biol. *21*, 319–329.

Feldmann, H.M., Golozoubova, V., Cannon, B., and Nedergaard, J. (2009). UCP1 ablation induces obesity and abolishes diet-induced thermogenesis in mice exempt from thermal stress by living at thermoneutrality. Cell Metab. *9*, 203–209.

Forner, F., Arriaga, E.A., and Mann, M. (2006a). Mild protease treatment as a small-scale biochemical method for mitochondria purification and proteomic mapping of cytoplasm-exposed mitochondrial proteins. J. Proteome Res. *5*, 3277–3287.

Forner, F., Foster, L.J., Campanaro, S., Valle, G., and Mann, M. (2006b). Quantitative proteomic comparison of rat mitochondria from muscle, heart, and liver. Mol. Cell. Proteomics *5*, 608–619.

Fraley, C., and Raftery, A.E. (2002). Model-based clustering, discriminant analysis, and density estimation. J. Am. Stat. Assoc. *97*, 611–631.

Fujino, T., Kondo, J., Ishikawa, M., Morikawa, K., and Yamamoto, T.T. (2001). Acetyl-CoA synthetase 2, a mitochondrial matrix enzyme involved in the oxidation of acetate. J. Biol. Chem. *276*, 11420–11426.

Gonzalez-Baro, M.R., Lewin, T.M., and Coleman, R.A. (2007). Regulation of triglyceride metabolism. II. Function of mitochondrial GPAT1 in the regulation of triacylglycerol biosynthesis and insulin action. Am. J. Physiol. Gastrointest. Liver Physiol. *292*, G1195–G1199.

Guarente, L. (2008). Mitochondria—a nexus for aging, calorie restriction, and sirtuins? Cell *132*, 171–176.

Hazen, S.A., Waheed, A., Sly, W.S., LaNoue, K.F., and Lynch, C.J. (1996). Differentiation-dependent expression of CA V and the role of carbonic anhydrase isozymes in pyruvate carboxylation in adipocytes. FASEB J. *10*, 481–490.

Holloway, G.P., Bonen, A., and Spriet, L.L. (2009). Regulation of skeletal muscle mitochondrial fatty acid metabolism in lean and obese individuals. Am. J. Clin. Nutr. *89*, 455S–462S.

Hubner, N.C., Ren, S., and Mann, M. (2008). Peptide separation with immobilized pI strips is an attractive alternative to in-gel protein digestion for proteome analysis. Proteomics *8*, 4862–4872.

Jakus, P.B., Sandor, A., Janaky, T., and Farkas, V. (2008). Cooperation between BAT and WAT of rats in thermogenesis in response to cold, and the mechanism of glycogen accumulation in BAT during reacclimation. J. Lipid Res. *49*, 332–339.

Katic, M., Kennedy, A.R., Leykin, I., Norris, A., McGettrick, A., Gesta, S., Russell, S.J., Bluher, M., Maratos-Flier, E., and Kahn, C.R. (2007). Mitochondrial gene expression and increased oxidative metabolism: role in increased lifespan of fat-specific insulin receptor knock-out mice. Aging Cell *6*, 827–839.

Klaus, S., Casteilla, L., Bouillaud, F., and Ricquier, D. (1991). The uncoupling protein UCP: a membraneous mitochondrial ion carrier exclusively expressed in brown adipose tissue. Int. J. Biochem. *23*, 791–801.

Klingenspor, M. (2003). Cold-induced recruitment of brown adipose tissue thermogenesis. Exp. Physiol. *88*, 141–148.

Kramarova, T.V., Shabalina, I.G., Andersson, U., Westerberg, R., Carlberg, I., Houstek, J., Nedergaard, J., and Cannon, B. (2008). Mitochondrial ATP synthase levels in brown adipose tissue are governed by the c-Fo subunit P1 isoform. FASEB J. *22*, 55–63.

Kratchmarova, I., Kalume, D.E., Blagoev, B., Scherer, P.E., Podtelejnikov, A.V., Molina, H., Bickel, P.E., Andersen, J.S., Fernandez, M.M., Bunkenborg, J., et al. (2002). A proteomic approach for identification of secreted proteins during the differentiation of 3T3-L1 preadipocytes to adipocytes. Mol. Cell Prot. *1*, 213–222.

Lambeth, D.O., Tews, K.N., Adkins, S., Frohlich, D., and Milavetz, B.I. (2004). Expression of two succinyl-CoA synthetases with different nucleotide specificities in mammalian tissues. J. Biol. Chem. *279*, 36621–36624.

Lattin, J.E., Schroder, K., Su, A.I., Walker, J.R., Zhang, J., Wiltshire, T., Saijo, K., Glass, C.K., Hume, D.A., Kellie, S., and Sweet, M.J. (2008). Expression analysis of G protein-coupled receptors in mouse macrophages. Immunome Res. *4*, 5. 10.1186/1745-7580-4-5.

Mann, M., and Kelleher, N.L. (2008). Precision proteomics: the case for high resolution and high mass accuracy. Proc. Natl. Acad. Sci. USA *105*, 18132–18138.

Mashek, D.G., Li, L.O., and Coleman, R.A. (2006a). Rat long-chain acyl-CoA synthetase mRNA, protein, and activity vary in tissue distribution and in response to diet. J. Lipid Res. *47*, 2004–2010.

Mashek, D.G., McKenzie, M.A., Van Horn, C.G., and Coleman, R.A. (2006b). Rat long chain acyl-CoA synthetase 5 increases fatty acid uptake and partitioning to cellular triacylglycerol in McArdle-RH7777 cells. J. Biol. Chem. *281*, 945–950.

Mootha, V.K., Bunkenborg, J., Olsen, J.V., Hjerrild, M., Wisniewski, J.R., Stahl, E., Bolouri, M.S., Ray, H.N., Sihag, S., Kamal, M., et al. (2003). Integrated analysis of protein composition, tissue diversity, and gene regulation in mouse mitochondria. Cell *115*, 629–640.

Moura, M.A., Festuccia, W.T., Kawashita, N.H., Garofalo, M.A., Brito, S.R., Kettelhut, I.C., and Migliorini, R.H. (2005). Brown adipose tissue glyceroneogenesis is activated in rats exposed to cold. Pflugers Arch. *449*, 463–469.

Nedergaard, J., Bengtsson, T., and Cannon, B. (2007). Unexpected evidence for active brown adipose tissue in adult humans. Am. J. Physiol. Endocrinol. Metab. *293*, E444–E452.

Ong, S.E., Blagoev, B., Kratchmarova, I., Kristensen, D.B., Steen, H., Pandey, A., and Mann, M. (2002). Stable isotope labeling by amino acids in cell culture, SILAC, as a simple and accurate approach to expression proteomics. Mol. Cell. Proteomics *1*, 376–386.

Pagliarini, D.J., Calvo, S.E., Chang, B., Sheth, S.A., Vafai, S.B., Ong, S.E., Walford, G.A., Sugiana, C., Boneh, A., Chen, W.K., et al. (2008). A mitochondrial protein compendium elucidates complex I disease biology. Cell *134*, 112–123.

Pan, C., Kumar, C., Bohl, S., Klingmueller, U., and Mann, M. (2009). Comparative proteomic phenotyping of cell lines and primary cells to assess preservation of cell type-specific functions. Mol. Cell. Proteomics *8*, 443–450.

Rappsilber, J., Ishihama, Y., and Mann, M. (2003). Stop and go extraction tips for matrix-assisted laser desorption/ionization, nanoelectrospray, and LC/MS sample pretreatment in proteomics. Anal. Chem. *75*, 663–670.

Rosen, E.D., and Spiegelman, B.M. (2006). Adipocytes as regulators of energy balance and glucose homeostasis. Nature *444*, 847–853.

Ross, T.K., Prahl, J.M., Herzberg, I.M., and DeLuca, H.F. (1992). Baculovirus-mediated expression of retinoic acid receptor type gamma in cultured insect cells reveals a difference in specific DNA-binding behavior with the 1,25-dihydroxyvitamin D3 receptor. Proc. Natl. Acad. Sci. USA *89*, 10282–10286.

Ryan, M.T., and Hoogenraad, N.J. (2007). Mitochondrial-nuclear communications. Annu. Rev. Biochem. *76*, 701–722.

Saito, M., Okamatsu-Ogura, Y., Matsushita, M., Watanabe, K., Yoneshiro, T., Nio-Kobayashi, J., Iwanaga, T., Miyagawa, M., Kameya, T., Nakada, K., et al. (2009). High incidence of metabolically active brown adipose tissue in healthy adult humans: effects of cold exposure and adiposity. Diabetes *58*, 1526–1531.

Sakakibara, I., Fujino, T., Ishii, M., Tanaka, T., Shimosawa, T., Miura, S., Zhang, W., Tokutake, Y., Yamamoto, J., Awano, M., et al. (2009). Fasting-induced hypothermia and reduced energy production in mice lacking acetyl-CoA synthetase 2. Cell Metab. *9*, 191–202.

Schwerzmann, K., and Pedersen, P.L. (1986). Regulation of the mitochondrial ATP synthase/ATPase complex. Arch. Biochem. Biophys. *250*, 1–18.

Seale, P., Bjork, B., Yang, W., Kajimura, S., Chin, S., Kuang, S., Scime, A., Devarakonda, S., Conroe, H.M., Erdjument-Bromage, H., et al. (2008). PRDM16 controls a brown fat/skeletal muscle switch. Nature *454*, 961–967.

Seale, P., Kajimura, S., and Spiegelman, B.M. (2009). Transcriptional control of brown adipocyte development and physiological function—of mice and men. Genes Dev. *23*, 788–797.

Stone, S.J., Levin, M.C., Zhou, P., Han, J., Walther, T.C., and Farese, R.V., Jr. (2009). The endoplasmic reticulum enzyme DGAT2 is found in mitochondria-associated membranes and has a mitochondrial targeting signal that promotes its association with mitochondria. J. Biol. Chem. *284*, 5352–5361.

Timmons, J.A., Wennmalm, K., Larsson, O., Walden, T.B., Lassmann, T., Petrovic, N., Hamilton, D.L., Gimeno, R.E., Wahlestedt, C., Baar, K., et al. (2007). Myogenic gene expression signature establishes that brown and white adipocytes originate from distinct cell lineages. Proc. Natl. Acad. Sci. USA *104*, 4401–4406.

Tiranti, V., Viscomi, C., Hildebrandt, T., Di Meo, I., Mineri, R., Tiveron, C., Levitt, M.D., Prelle, A., Fagiolari, G., Rimoldi, M., and Zeviani, M. (2009). Loss of

ETHE1, a mitochondrial dioxygenase, causes fatal sulfide toxicity in ethylmalonic encephalopathy. Nat. Med. *15*, 200–205.

Turner, N., and Heilbronn, L.K. (2008). Is mitochondrial dysfunction a cause of insulin resistance? Trends Endocrinol. Metab. *19*, 324–330.

Uldry, M., Yang, W., St-Pierre, J., Lin, J., Seale, P., and Spiegelman, B.M. (2006). Complementary action of the PGC-1 coactivators in mitochondrial biogenesis and brown fat differentiation. Cell Metab. *3*, 333–341.

van Marken Lichtenbelt, W.D., Vanhommerig, J.W., Smulders, N.M., Drossaerts, J.M., Kemerink, G.J., Bouvy, N.D., Schrauwen, P., and Teule, G.J. (2009). Cold-activated brown adipose tissue in healthy men. N. Engl. J. Med. *360*, 1500–1508.

Virtanen, K.A., Lidell, M.E., Orava, J., Heglind, M., Westergren, R., Niemi, T., Taittonen, M., Laine, J., Savisto, N.J., Enerback, S., and Nuutila, P. (2009). Functional brown adipose tissue in healthy adults. N. Engl. J. Med. *360*, 1518–1525.

Waki, H., and Tontonoz, P. (2007). Endocrine functions of adipose tissue. Annu. Rev. Pathol. *2*, 31–56.

Watkins, P.A., Maiguel, D., Jia, Z., and Pevsner, J. (2007). Evidence for 26 distinct acyl-coenzyme A synthetase genes in the human genome. J. Lipid Res. *48*, 2736–2750.

Wendel, A.A., Lewin, T.M., and Coleman, R.A. (2008). Glycerol-3-phosphate acyltransferases: rate limiting enzymes of triacylglycerol biosynthesis. Biochim. Biophys. Acta *1791*, 501–506.

Yates, J.R., 3rd, Gilchrist, A., Howell, K.E., and Bergeron, J.J. (2005). Proteomics of organelles and large cellular structures. Nat. Rev. Mol. Cell Biol. *6*, 702–714.

Yu, X.X., Lewin, D.A., Forrest, W., and Adams, S.H. (2002). Cold elicits the simultaneous induction of fatty acid synthesis and beta-oxidation in murine brown adipose tissue: prediction from differential gene expression and confirmation in vivo. FASEB J. *16*, 155–168.